IEEE Transactions on Nuclear Science, Vol. NS-30, No. 4, August 1983 

# LOW MOMENTUM KAON BEAM LINES

D.E. Lobb

TRIUMF, Physics Department, University of Victoria
Victoria, B.C., Canada V8W 2Y2

## Summary

Current low momentum ($\lesssim$ 500 MeV/c) high acceptance ($\lesssim$ 5 msr) kaon beam lines feature high ratios of charged contaminant particles to kaons. The results of computer calculations on scattering and pion production from $K^0_S$ decay are presented to indicate some of the sources of this contamination. Criteria for the design of beam lines are discussed and a new beam line design is proposed.

## Introduction

Low momentum kaon beam lines at present accelerator facilities are as short as possible in order to provide an acceptable flux of kaons at an experimental location. Design studies are now underway for accelerators that would provide primary proton beam currents 100 to 1000 times greater than those provided by present accelerators[1, 2]. At such a facility, the total number of events per second in an experiment way well exceed the capabilities of the data collection and analysis systems. It then becomes imperative to reduce the number of events caused by contaminant particles. There is considerable scope for improvement in beam purity: contaminant particle to kaon ratios as large as 50:1 have been reported[3].

In Table 1 we present some relative cross sections and some contamination ratios at the production target. These contamination ratios are enhanced by the different decay rates for the particles traveling down a channel. In Table 2 we present the ratio of the surviving fraction of pions to the surviving fraction of kaons as a function of the particle energy and the distance from the production target. In the absence of mass selection, the $\pi^-/K^-$ ratio at the end of a channel of practical length is $\sim$ 2000. This presents a stringent criterion for the quality of a channel: for a $\pi^-/K^-$ ratio of 1:1, the channel must transmit only $\lesssim$ 0.2% of the pions which originally overlapped the accepted kaon phase space.

Table 1. Calculated relative production cross sections and pion to kaon production ratios for $0.49 \leq p \leq 0.51$ GeV/c particles into an elliptical angular acceptance with half axes of 100 mrad in the zx plane and 10 mrad in the yz plane (3.1 msr). The results were obtained by a Monte-Carlo integration of the Sanford-Wang formula[4,5,6,7] including kinematic reflection[8,9]. The $K^-$ cross section for 12 GeV protons is set equal to unity.

| Proton beam energy (GeV) | $K^-$ | $\pi^-$ | $\pi^-/K^-$ | $K^+$ | $\pi^+$ | $\pi^+/K^+$ |
|---|---|---|---|---|---|---|
| 12 | 1.00 | 204. | 204. | 3.06 | 243. | 80. |
| 18 | 1.09 | 266. | 244. | 2.69 | 304. | 113. |
| 24 | 1.17 | 324. | 276. | 2.46 | 370. | 151. |

Table 2. The ratio of the surviving fraction of pions to the surviving fraction of kaons.

| Distance from production target (m) | Momentum (GeV/c) 0.5 | 0.7 | 1.1 |
|---|---|---|---|
| 10 | 10.0 | 5.2 | 2.8 |
| 12 | 15.9 | 7.2 | 3.5 |
| 14 | 25.2 | 10.0 | 4.3 |
| 16 | 39.9 | 13.9 | 5.3 |
| 18 | 63.3 | 19.4 | 6.6 |

For particles originating within the primary proton beam spot on the target, practical electrostatic separators can cleanly separate the phase space of $\sim$ 0.5 GeV/c kaons from the phase spaces of the contaminant pions, muons and electrons. In the following sections we present results for the processes of $K^0_S$ decay and pion scattering which give rise to pion trajectories that form a halo around the direct beam. In the final section we present a design for a 0.55 GeV high purity kaon channel. The reader is also referred to the criteria for design and the proposed channel presented by Berien[3], and the channels proposed by Thiessen[10], Enge[11] and Lobb[12].

## Pions Produced by $K^0_S$ Decay

The $K^0_S$ particle has a very short half life resulting in decays very close to the production target: after a 1 m drift the survival of 5 and 10 GeV/c $K^0_S$ is only 2.4% and 15.6% respectively. The dominant decay mode (68.61%) is $K^0 \rightarrow \pi^+ \pi^-$: the decay products are referred to as cloud pions. In Table 3 we present results obtained using a Monte Carlo program[12] to calculate the effective ratios at the plane of the production target of cloud pions to $\pi^\pm$ and $K^\pm$. For $0.4 \leq p \leq 0.6$ GeV/c particles these results indicate a cloud pion to $K^-$ ratio $\sim$ 1.5:1 at the production target which would be enhanced to a ratio $\sim$ 24:1 after a 12 m drift. However, the effective source size is large: for $0.4 \leq p \leq 0.6$ GeV/c, 68% lie outside a 1 cm radius disc, 48% lie outside a 2 cm radius disc, and 10% lie outside an 8 cm radius disc. A mass slit located at a dispersed horizontal focus images back to the target plane as a horizontal strip. If, for example, this image for pions is $1 \leq y \leq 3$ cm, only 14% of the effective cloud pion source lies within the image of the mass slit, resulting in a cloud pion to $K^-$ ratio of $\sim$ 3:1 at the end of a 12 m channel. Therefore, while cloud pions are a significant source of contamination, they are not the major contributor to $\pi^-/K^-$ ratios $\gtrsim$10:1.

## Glancing Angle Scattering

If the aperture of a focussing element defines the angular acceptance of the channel, many of the rays that strike the aperture do so at a small angle; for example, if a 50$\pi$ cm·mrad emittance occupies an aperture of 10 cm half width, the angles of the trajectories with respect to the element axis are $\leq$ 5 mrad. Rays lying outside this emittance will strike the aperture somewhere inside the focussing element.

The program REVMOC[14] has been used to investigate what happens when a pencil beam strikes a plane surface at a glancing angle. This program performs Monte Carlo calculations for multiple and nuclear scattering. (These calculations are not available inside a magnetic field so the actual problem of rays reaching a maximum distance from the central trajectory inside a focussing element cannot be modelled accurately.) Results are presented for copper and iron in Table 4; the basic geometry is illustrated in Fig. 1. The incoming rays lie in a zx plane while the material boundary lies in a yz plane. The rays that exit the material through this boundary (that are "reflected") make an angle $\phi$ with respect to the zx plane. Calculations have been performed for 0.5 GeV/c charged pions. The program keeps track of the longitudinal bin in which the first and last scattering events occur; the latter defines the point of exit of the ray from the material.

0018-9499/83/0800-2827$01.00©1983 IEEE

Table 3. The effective ratio at the plane of the production target of pions produced from $K^0_S$ decay (labelled cp) to $\pi^{\pm}$ and $K^{\pm}$ for 25 GeV/c proton momentum and an angular acceptance of 50 mrad half angle (7.8 msr). Also presented are the $\pi^+/K^+$ and $\pi^-/K^-$ ratios for direct production.

| p(GeV/c) | $cp/\pi^+$ | $cp/\pi^-$ | $cp/K^+$ | $cp/K^-$ | $\pi^+/K^+$ | $\pi^-/K^-$ |
|---|---|---|---|---|---|---|
| 0.4 → 0.6 | 0.006 | 0.007 | 0.73 | 1.52 | 122. | 215. |
| 0.6 → 0.8 | 0.009 | 0.010 | 0.73 | 1.33 | 83. | 126. |
| 0.8 → 1.0 | 0.013 | 0.016 | 0.77 | 1.38 | 59. | 86. |
| 1.0 → 1.2 | 0.014 | 0.018 | 0.62 | 1.15 | 43. | 63. |
| 1.2 → 1.4 | 0.018 | 0.023 | 0.58 | 1.14 | 32. | 49. |
| 1.4 → 1.6 | 0.017 | 0.022 | 0.42 | 0.86 | 24. | 38. |
| 1.6 → 1.8 | 0.016 | 0.021 | 0.29 | 0.64 | 18. | 31. |
| 1.8 → 2.0 | 0.015 | 0.020 | 0.25 | 0.55 | 16. | 27. |

Fig. 1. The geometry for glancing angle scattering; p refers to the component of $\vec{p}$ normal to $p_z$.

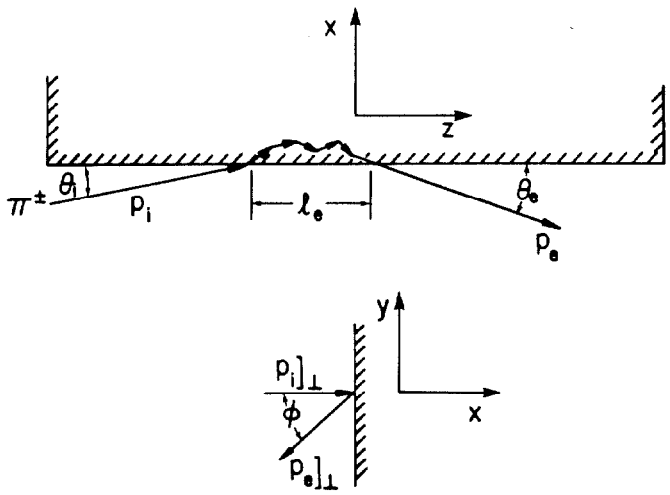


Table 4. Glancing-angle scattering for 0.5 GeV/c charged pions incident on 6 cm of iron and copper.

| $\theta_i$ (mrad) | Percent Reflected Back: Total | Nuclear Scatter | Multiple Scatter | $\bar{\ell}_e$ (cm): Nuclear Scatter | Multiple Scatter | $\bar{\theta}_e$ (mrad) | $\theta_e)_{rms}$ (mrad) | $\overline{(\theta_e-\theta_i)}$ (mrad) | $(\theta_e-\theta_i)_{rms}$ (mrad) | $\phi_{rms}$ (mrad) | $\overline{(\frac{\Delta p}{p})}$ (%) | $(\frac{\Delta p}{p})_{rms}$ (%) |
|---|---|---|---|---|---|---|---|---|---|---|---|---|
| | | | | | | RESULTS FOR IRON | | | | | | |
| 10 | 51.1 | 5.7 | 45.4 | 2.6 | 1.3 | -31.7 | 48.4 | -77.5 | 85.6 | 45.7 | -3.9 | 5.5 |
| 20 | 35.6 | 7.1 | 28.5 | 2.7 | 2.0 | -45.4 | 62.7 | -65.4 | 78.4 | 57.4 | -5.7 | 7.1 |
| 30 | 25.4 | 7.0 | 18.4 | 2.8 | 2.6 | -57.4 | 74.6 | -87.4 | 99.6 | 66.7 | -7.2 | 8.3 |
| 40 | 18.3 | 6.5 | 11.8 | 3.0 | 3.0 | -65.1 | 81.9 | -105.2 | 116.3 | 72.0 | -8.1 | 9.2 |
| 50 | 12.9 | 5.8 | 7.0 | 3.0 | 3.5 | -76.7 | 93.2 | -126.7 | 137.4 | 79.8 | -8.8 | 9.9 |
| | | | | | | RESULTS FOR COPPER | | | | | | |
| 10 | 50.1 | 5.8 | 44.4 | 2.7 | 1.4 | -30.3 | 47.4 | -40.3 | 54.4 | 44.8 | -3.7 | 5.2 |
| 20 | 32.8 | 6.4 | 26.4 | 2.8 | 2.2 | -44.6 | 63.0 | -64.6 | 78.4 | 56.3 | -5.6 | 6.8 |
| 30 | 22.6 | 6.3 | 16.2 | 2.9 | 2.8 | -56.7 | 74.4 | -86.7 | 99.2 | 66.7 | -6.9 | 7.9 |
| 40 | 16.0 | 6.2 | 9.8 | 3.1 | 3.2 | -68.4 | 86.1 | -108.4 | 120.3 | 74.8 | -7.8 | 8.7 |
| 50 | 11.1 | 5.2 | 5.9 | 3.1 | 3.6 | -78.5 | 96.4 | -128.5 | 140.2 | 77.7 | -8.2 | 9.2 |

From Table 4 it can be seen that for 10 mrad angle of incidence, ∿ 50% of the rays are reflected back; even for 50 mrad angle of incidence a substantial number (∿ 10%) are reflected back. The nuclear scattered rays emerge fairly uniformly along the length considered; the multiple scattered rays emerge near the point of incidence for small angles of incidence and fairly uniformly along the length considered for larger angles of incidence. The change in the direction of the emergent rays in the plane of incidence is about twice the change in direction normal to the plane of incidence. The momentum loss for reflected rays is ∿ 5% to ∿ 10%.

For rays initially in a horizontal plane, the large phase space acceptance in this plane will result in some of these rays being accepted by the downstream system. The scattering in the vertical direction for these rays will result in a halo being formed about the vertical beam spot at the mass slit. Referring back to the comment that a number of pions equivalent to ∿ 0.2% of the pions coming directly from the target will result in a $\pi^-/K^-$ ratio ∿ 1:1 at the end of a channel, we see that trajectories just adjacent to the accepted phase space and trajectories with an initial higher momentum whose momentum loss brings them down into the system momentum acceptance band can easily provide the required number of pions to produce the observed levels of contamination. It is clear that the system phase space acceptance must be defined by slits and collimators and not by the vacuum chamber inside a focussing element.

## A Proposed High Purity 0.55 GeV/c Kaon Beam Line

The features of this design are slits located to define the phase space acceptance and a separator section that has an object-image relationship between two achromatic stigmatic foci. Design calculations were performed using TRANSPORT[14].

The channel consists of three parts (see Fig. 2). The 5.6 m long first section, from the production target to the achromatic stigmatic focus at FHV1, defines the beam emittance. Midway within this section a horizontal slit located along the tilted horizontal focal plane defines the momentum acceptance and a vertical slit defines the vertical angular acceptance off the target. A sextupole

(2.5 kG at 12.0 cm radius, 0.2 m long) at this location is used to set $y|\phi_0\delta = 0$ at the mass slit downstream (location FHV2). The uniform field wedge bending magnets have 14.4 kG across a vertical gap of 7 cm; the effective length is 1.0 m. A collimator at FHV1 defines the x,y and $\theta$ phase space transmission.

Fig 2. A proposed 0.55 GeV/c kaon channel.

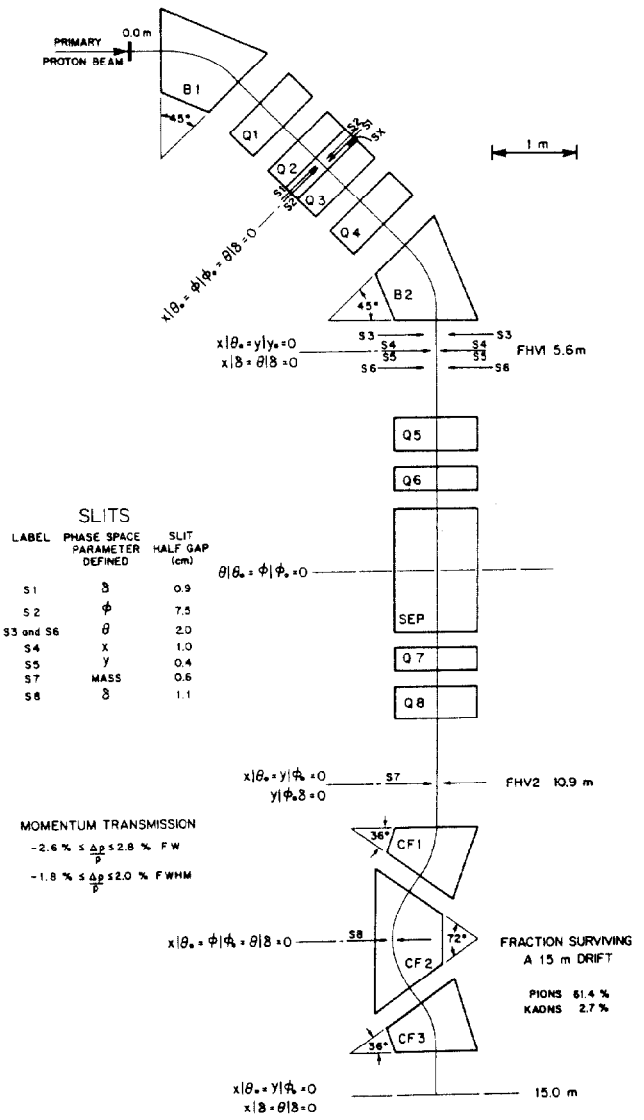


Table 5. Quadrupole parameters for the $\bar{s}$ystem presented in Fig. 2.

| | Quadrupole Pole Tip Field (kG) | Effective Length (m) | Aperture Radius (cm) |
|---|---|---|---|
| Q1 | 11.5 | 0.4 | 14.0 |
| Q2 | -7.9 | 0.3 | 12.0 |
| Q3 | -7.9 | 0.3 | 12.0 |
| Q4 | 11.5 | 0.4 | 14.0 |
| Q5 | 11.1 | 0.4 | 12.0 |
| Q6 | -7.7 | 0.3 | 10.0 |
| Q7 | -7.7 | 0.3 | 10.0 |
| Q8 | 11.1 | 0.4 | 12.0 |

The 5.3 m long separator section between FHV1 and the mass slit at the stigmatic focus FHV2 contains a 1.5 m long separator operated with 0.98 MV across 14 cm plate separation (70.3 kV/cm) providing a 6.0 mrad angular separation between the pion and kaon central trajectories. TURTLE[16] calculations indicate a clean separation of the two beam spots: the kaon beam lying within the limits $-0.65 \leqq y \leqq 0.65$ cm and the pion beam lying within the limits $1.05 \leqq y \leqq 2.30$ cm.

The 4.1 m long third section delivers the beam to the experimental location. Since this section should be as short as possible, we have used combined function magnets (suggested by Yamamoto[17]) in which the dipole and quadrupole components of the field are produced by independent superconducting current sheets. The wedge magnets CF1 and CF3 have 18.0 kG across 10 cm vertical gap, an n-value of -3.23 and an effective length of 0.64 m; CF2 has 18.0 kG across 18 cm vertical gap, an n-value of 1.68 and an effective length of 1.28 m. A slit is located at the middle of element CF2 to remove particles that have left the momentum range of the direct beam due to energy loss at upstream slits.

The total length of the channel is 15.0 m resulting in 2.7% survival of 0.55 GeV/c charged kaons and 61.4% survival of 0.55 GeV/c charged pions. The momentum transmission of the system is $-2.6\% \leqq \Delta p/p \leqq 2.8\%$ full width and $-1.8\% \leqq \Delta p/p \leqq 2.0\%$ full width half height. Most of the beam is within a circle 1.5 cm radius at the achromatic stigmatic focus at the end of the channel.

## Conclusions

The processes of cloud pion production and glancing angle scattering produce a halo around the beam that originates directly from the production target. An achromatic intermediate focus will remove such particles from the transmitted beam. The improved purity of the kaon beam will, under some circumstances, compensate for the loss of flux due to increased length of such a channel compared to a channel which has been designed to be as short as possible.

## Acknowledgements

The author wishes to thank A.K.C. Chan for writing the program to perform the cloud pion Monte Carlo calculations, and P. Berien for helpful discussions.

## References

1. M.K. Craddock, Proc. of the Int. Conf. on Hypernuclear and Kaon Physics (1982) 389; LAMPF report LA-9572-C (1982)43; this conference, Paper B6 ('83)
2. H.A. Thiessen, Proc. of the Int. Conf. on Hypernuclear and Kaon Physics (1982) 399; LAMPF report LA-9572-C (1982) 12
3. P. Berien, Proc. of the Int. Conf. on Hypernuclear and Kaon Physics (1982) 371
4. J.R. Sanford and C.L. Wang, BNL 11279 (1967)
5. J.R. Sanford and C.L. Wang, BNL 11479 (1967)
6. C.L. Wang, Phys. Rev. Lett. 25 (1970) 1068
7. C.L. Wang, BNL 17218 (1972)
8. M. Zeller et al., BNL 16000 (1970) 193
9. D. Berley, BNL 50579 (1976) 257
10. H.A. Thiessen, LA-8775-C (1981) 487
11. H. Enge, LA-9416-C (1982) 34
12. D.E. Lobb, LA-9416-C (1982) 30
13. D.E. Lobb, TRIUMF report VPN-82-6 (1983)
14. C. Kost and P.A. Reeve, TRI-DN-82-28 (1982)
15. K.L. Brown et al., CERN 80-04 (1980)
16. K.L. Brown and Ch. Iselin, CERN 74-2 (1974)
17. A. Yamamoto et al., TRI-79-1 (1979)